

Optimisation and analysis of efficiency for contra-rotating propellers for high-altitude airships

J. Tang , X. Wang, D. Duan, W. Xie

tangjw@stju.edu.cn

School of Aeronautics and Astronautics
Shanghai Jiao Tong University
Shanghai, China

ABSTRACT

An improved variational optimization approach is established to optimize and analyse the propulsion efficiency of the high-altitude contra-rotating propellers for high-altitude airships based on the Vortex Lattice Lifting Line Method. The optimum radial circulation distribution, chord and pitch distribution are optimized under the maximum lift-to-drag ratio of aerofoils. To consider the effects of the actual Reynolds number and the Mach number of each aerofoil section, aerodynamics such as lift coefficient, drag coefficient and lift-to-drag ratio are obtained by interpolating a CFD database, which is established by numerical simulations under different Reynolds number, Mach number and angles-of-attack. The improved method is verified by validation cases on a high-altitude CRP using the three-dimensional steady Reynolds-averaged Navier-Stokes solver and moving reference frames technique. The optimization results of thrust, torque and efficiency for both the individual front/rear propeller and CRP are shown to agree reasonably well with the CFD results. Using the improved approach, the influence of blade numbers, diameter, rotation speeds, axial distance and torque ratio on the optimum efficiency of CRPs is illustrated in detail by conducting parametric studies.

Keywords: High-altitude airships; Contra-rotating propellers; Optimization; Analysis; Efficiency

NOMENCLATURE

Z	blade number
D	diameter of propeller disk, m
d	spacing between the forward propeller and rear propellers, m
X_f	axial distance ratio
R	radius of propeller, m
r	radius to the blade element, m

c	chord length, m
V_a	axial inflow velocity, m/s
V_t	tangential inflow velocity, m/s
N	rotation speed (per minute), r/min
n	rotation speed (per second), r/s
ω	angular rotation speed, rad/s
C_L	lift coefficient
C_D	drag coefficient
Re	Reynolds number
Ma	Mach number
Γ	circulation
u_a^*	axial-induced velocity, m/s
u_t^*	tangential-induced velocity, m/s
q	torque ratio, (Q_2/Q_1)
λ_T	Lagrange multipliers for thrust
λ_Q	Lagrange multipliers for torque
ρ	air density, kg/m^3
μ	dynamic viscosity, $kg/(m \cdot s)$
J_S	advance ratio
T	thrust of propeller, N
Q	torque of propeller, $N \cdot m$
KT	thrust coefficient
KQ	torque coefficient
η	propeller efficiency, %
V_{a_j}	axial inflow velocity
V_{t_j}	tangential inflow velocity
$u_{a_j,j}^*$	axial self-induced velocity on component j
$u_{a_j,k}^*$	interaction-induced velocity on component j
$u_{t_j,j}^*$	tangential self-induced velocity on component j
$u_{t_j,k}^*$	interaction-induced velocity on component j
V_j^*	resultant velocity on component j
β_j	inflow angle
β_{ij}	aerodynamic pitch angle
α_j	angle-of-attack
θ_j	pitch angle of the aerofoil
T_j	thrust force of the aerofoil
D_j	tangential force of the aerofoil
F_{v_j}	inviscid lift force
F_{i_j}	viscous force
F_j	resultant force
$j(n)$	the n_{th} control point on propeller j
$u_{a_j(n)}^*$	axial-induced velocity induced by the individual horseshoe vortices
$u_{t_j(n)}^*$	tangential-induced velocity induced by the individual horseshoe vortices
$\bar{u}_{a_j,k}^*(n, m)$	axial velocity-induced factors at the n_{th} control point of propeller j by horseshoe vortex of unit strength at the m_{th} control point of propeller k

$\bar{u}_{i,j,k}^*$ (n, m)	tangential velocity-induced factors at the n_{th} control point of propeller j by horseshoe vortex of unit strength at the m_{th} control point of propeller k
Γ_k (m)	circulation at the m_{th} control point of propeller k
$(L/D)_{\max}$	maximum lift-drag ratio
c_a	local air velocity.

Subscript

j	the number of propellers ($j = 1, j = 2$ represents the forward and rear propeller, respectively)
I	inviscid terms
V	viscous terms

1.0 INTRODUCTION

In recent years, the high-altitude airships (HAAs) have received widespread attention in the aerospace sciences. The long endurance, low energy consumption and high security make HAAs attractive both in the military and civilian areas^(1,2). The above features rely on a high-efficiency propulsion system. Until now, the propeller propulsion systems have been widely used in HAAs⁽³⁾.

HAAs usually fly at about 20–30 km, where the environment is much different from that of low altitude. Therefore, the propeller operates under much lower air density, resulting in a low Reynolds number. Besides, the advance velocity is extremely low (about 10–30m/s). The above two factors make it difficult to achieve the same efficiency level as conventional propellers operating at relatively low altitude⁽⁴⁾. Therefore, improving the propeller efficiency as much as possible has become a key problem⁽⁵⁾. Based on conventional single propeller configurations, techniques such as co-flow jet flow control⁽⁶⁾, plasma⁽⁷⁾ and proplet⁽⁸⁾ techniques have been adopted to improve the propeller efficiency. However, the effects were found to be limited. Therefore, the concept of the contra-rotating propeller (CRP) was proposed for HAAs⁽⁹⁾, which consists of two coaxial propellers positioned a short distance apart and rotating in opposite directions. Fig. 1 shows the simplified configuration of high-altitude contra-rotating propellers.

Many investigations on CRPs have been conducted in the last several decades, but mainly focused on the application on the vessel or airplane. Higher efficiency of CRPs over single propellers at low altitude has been validated^(10,11), mainly due to the recovery of the rotational energy losses originating from the forward propeller by the counter-rotating rear propeller⁽¹²⁾. For example, wind tunnel tests conducted by Biermann and Hartman⁽¹³⁾ showed that the contra-rotating propeller achieved higher power absorption and efficiency than a single propeller. McHugh and Pepper⁽¹⁴⁾ found that the aerodynamically improved airfoil designs highly affect the performance of CRPs. But few of the above studies aimed at the applications at the operating conditions of low Reynolds number and small advance ratio. Recently, Tang et al. carried out wind tunnel tests for a stratospheric airship CRP scaling model (diameter of 0.75 m) and showed that the counter-rotating propeller would be a wise option applied on stratospheric airships⁽⁹⁾.

Similar to the single propeller design, the CRP design also aims to obtain the best parameter adjustments for the front and rear propellers. The parameters of a CRP include blade

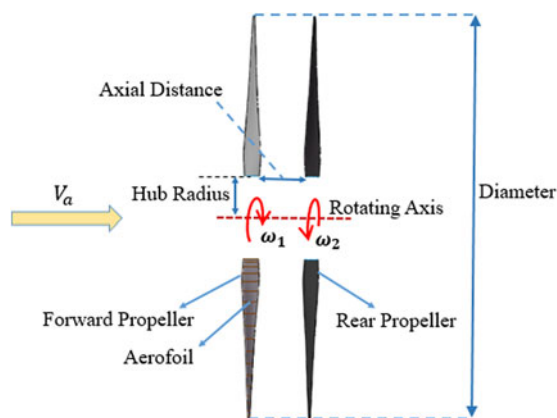


Figure 1. Simplified configuration of high-altitude contra-rotating propellers.

number, diameter, individual rotation speed for both propellers, axial distance, radial variation of cross-sectional profile shape, pitch angle, and chord length. However, due to the interference of the front and rear propellers, the maximum individual efficiency of the front or rear propeller does not necessarily mean the most desired CRP total efficiency. Therefore, the design of CRPs requires the coupling of optimization of the front and rear propellers.

Over the years, the Vortex Lattice Lifting Line Method (VLM) has been a commonly used method of designing propellers. This method gives a good prediction of the air propeller efficiency with large blade aspect ratios^(15–17). The first lifting line method for CRP was proposed by Lerbs⁽¹⁸⁾. His approach was an extension of the single propeller lifting line considering the interaction velocities induced by each propeller on the other. The blade numbers for the forward and the rear propellers were assumed the same. Lerbs' theory was then developed by Morgan and Wrench^(19,20) with the extension of any combination of blade numbers and derivation of accurate equations to compute the interactive induced velocities. They designed the CRPs by coupling two single propellers' code in an iterative way, which was actually an 'uncoupled' method. Kerwin et al.⁽²¹⁾ proposed a 'coupled' method, considering the CRP as an integrated propulsive unit and giving an iterative procedure to calculate the optimum circulation distribution at each propeller. The generalized numerical CRP variational optimizer for the 'uncoupled' and 'coupled' method was implemented by Laskos⁽²²⁾. Kravitz established an off-design analysis procedure to predict the performance for a given CRP, which was an extension of the single propeller off design analysis proposed by Epps⁽²³⁾.

However, the above methods did not consider the effects of the Reynolds number and Mach number on aerofoil at different radial locations, which significantly affect the performance of high-altitude CRPs. Besides, the chord length distributions were assumed the same for both propellers and were not part of the propeller circulation optimization process. However, as shown in the single propeller optimization study conducted by Zheng et al.⁽²⁴⁾, by taking into account the viscous effects of the chord length and optimizing the chord length distribution, higher efficiency of the single propeller can be achieved. Therefore, there is a need to introduce the individual chord length distributions for each propeller as optimized variables in the coupling optimization process for the high-altitude CRPs. Furthermore, as there is interference between the front and rear propellers, which is different from that of the high-altitude single propeller, the investigations on how the parameters such as blade numbers, diameter,

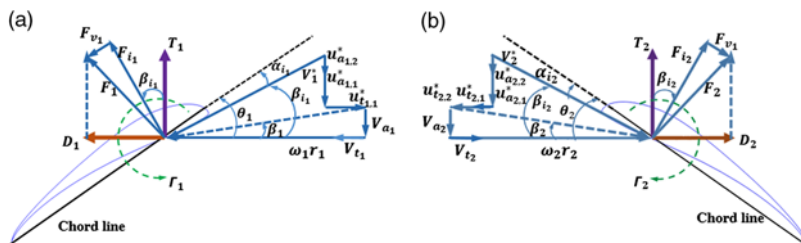


Figure 2. Velocity, angle and forces diagram of the CRP blade aerofoil: (a) Forward propeller. (b) Rear propeller.

rotation speeds, axial distance and torque ratio affect the optimum CRP efficiency need to be conducted as well.

The aim of this study is to develop an improved efficient variational optimization method for high-altitude CRPs based on the Kerwin's CRP optimizer⁽²¹⁾, which can consider the chord length distribution optimization and effects of the Reynolds number and the Mach number of aerofoil and investigate the effects of parameters on the optimum efficiency of high-altitude CRPs in detail. The desired circulation distribution, chord and pitch distribution are obtained under the maximum lift-to-drag ratio of aerofoils. The aerofoil aerodynamics data used in the iterative optimization process, such as lift, drag coefficient and lift-to-ratio, are obtained by interpolating a CFD database, which was established by numerical simulations for the different Reynolds number, Mach number and angles-of-attack. Therefore, the effects of the Reynolds number and the Mach number can be considered. The improved method is validated by using the three-dimensional steady Reynolds-averaged Navier-Stokes (RANS) solver and moving reference frames (MRF) technique. Using the improved approach, parametric studies are conducted in detail to illustrate how the optimum efficiency of high-altitude CRPs is influenced by the parameters of blade numbers, diameter, rotation speeds, the axial distance and torque ratio.

The paper is organized as follows. First, the improved algorithms for the contra-rotating propeller optimizer will be described in Section 2.0. Then, in Section 3.0, the validations are conducted by comparing the present results with the CFD data. In Section 4.0, the effects of parameters on the optimum CRP efficiency are investigated in detail. Last, in Section 5.0, the conclusions will be drawn.

2.0 METHODOLOGY

The velocity, angle and forces diagram of the blade aerofoil for both propellers are shown in Fig. 2. As the slipstream is assumed purely axial (no contraction of the incoming streamtube), the radial interaction velocity is set to zero.

The total thrust T and torque Q of the CRP are:

$$T = \sum_{j=1}^2 \{T_j\} = \sum_{j=1}^2 \{T_{I_j} + T_{V_j}\} \quad \dots (1)$$

$$Q = \sum_{j=1}^2 \{Q_j\} = \sum_{j=1}^2 \{Q_{I_j} + Q_{V_j}\} \quad \dots (2)$$

where

$$T_{I_j} = \rho Z_j \sum_{n=1}^{M_j} \left[\left(\omega_j r_{j(n)} + V_{t_{j(n)}} + u_{t_{j(n)}}^* \right) \cdot \Gamma_{j(n)} \Delta r_{j(n)} \right] \quad \dots (3)$$

$$T_{V_j} = -\frac{1}{2} \rho Z_j \sum_{n=1}^{M_j} \left[V_{j(n)}^* \cdot C_{D_{j(n)}} c_{j(n)} \left(V_{a_{j(n)}} + u_{a_{j(n)}}^* \right) \Delta r_{j(n)} \right] \quad \dots (4)$$

$$Q_{I_j} = \rho Z_j \sum_{i=1}^{M_j} \left[\left(V_{a_{j(n)}} + u_{a_{j(n)}}^* \right) \Gamma_{j(n)} r_{j(n)} \Delta r_{j(n)} \right] \quad \dots (5)$$

$$Q_{V_j} = \frac{1}{2} \rho Z_j \sum_{n=1}^{M_j} \left[V_{j(n)}^* C_{D_{j(n)}} c_{j(n)} \left(\omega_j r_{j(n)} + V_{t_{j(n)}} + u_{t_{j(n)}}^* \right) r_{j(n)} \Delta r_{j(n)} \right] \quad \dots (6)$$

And $u_{a_{j(n)}}^*$ and $u_{t_{j(n)}}^*$ can be written as:

$$u_{a_{j(n)}}^* = \sum_{k=1}^K \sum_{m=1}^{M_k} \Gamma_k(m) \cdot \bar{u}_{a_{j,k}}^*(n, m) \quad \dots (7)$$

$$u_{t_{j(n)}}^* = \sum_{k=1}^K \sum_{m=1}^{M_k} \Gamma_k(m) \cdot \bar{u}_{t_{j,k}}^*(n, m) \quad \dots (8)$$

where $\bar{u}_{a_{j,k}}^*(n, m)$ and $\bar{u}_{t_{j,k}}^*(n, m)$ can be calculated by the wake alignment model⁽¹⁷⁾.

Therefore, the propulsive efficiency of CRP can be written as:

$$\eta = \frac{\sum_{j=1}^2 (T_j V_a)}{\sum_{j=1}^2 (Q_j \omega_j)} \quad \dots (9)$$

In this paper, V_a is assumed to be equal to the advance speed of the airship V_s .

For a given total thrust T_r and the specific torque ratio $q = \frac{Q_2}{Q_1}$ to achieve the maximum efficiency, an auxiliary function H is formed by introducing two Lagrange multipliers λ_T , λ_Q ⁽²¹⁾:

$$H = (\omega_1 Q_1 + \omega_2 Q_2) + \lambda_T (T_1 + T_2 - T_r) + \lambda_Q (q Q_1 - Q_2) \quad \dots (10)$$

If $T_1 + T_2 = T_r$, $q Q_1 = Q_2$, then the minimal H is obtained as $H_{\min} = (\omega_1 Q_1 + \omega_2 Q_2)$, and the derivatives of H with respect to the unknown circulation values and Lagrange multipliers are set to be zero,

$$\frac{\partial H}{\partial \Gamma_{j(n)}} = 0 \quad \text{For } j = 1, 2; n = 1, \dots, M_j \quad \dots (11)$$

$$\frac{\partial H}{\partial \lambda_T} = 0 \quad \dots (12)$$

$$\frac{\partial H}{\partial \lambda_Q} = 0 \quad \dots (13)$$

Then, a system of $M_1 + M_2 + 2$ nonlinear equations with the same number of unknown variables can be obtained. This nonlinear problem can be linearized by freezing parameters u_{aj}^* , u_{tj}^* , $\bar{u}_{aj,k}^*$, $\bar{u}_{tj,k}^*$, V_j^* , λ_T , and λ_Q and iteratively solved by updating them at each iteration. And then the circulation distribution can be obtained. More details can be found in Kerwin⁽²¹⁾.

Using the convergent optimum circulation $\Gamma_{j(n)}$ and resultant velocity $V_{j(n)}^*$, and assuming all aerofoil sections working at the maximum lift-drag ratio $(L/D)_{\max} \cdot c_{j(n)}$ can be obtained as:

$$c_{j(n)} = \frac{2\Gamma_{j(n)}}{V_{j(n)}^* \cdot C_{L_{j(n)}-(L/D)_{\max}}} \quad \dots (14)$$

Substituting Equation (14) and the $C_{D_{j(n)}-(L/D)_{\max}}$ into Equations (4) and (6), T_{V_j} and Q_{V_j} can be rewritten as:

$$T_{V_j} = -\rho Z_j \sum_{n=1}^{M_j} \left[\frac{(V_{aj(n)} + u_{aj(n)}^*)}{(L/D)_{\max}} \cdot \Gamma_{j(n)} \Delta r_{j(n)} \right] \quad \dots (15)$$

$$Q_{V_j} = \rho Z_j \sum_{i=1}^{M_j} \left[\frac{(\omega_j r_{j(n)} + V_{tj(n)} + u_{tj(n)}^*)}{(L/D)_{\max}} \cdot \Gamma_{j(n)} r_{j(n)} \Delta r_{j(n)} \right] \quad \dots (16)$$

Now the systems can be linearized by freezing parameters u_{aj}^* , u_{tj}^* , \bar{u}_{aj}^* , \bar{u}_{tj}^* , $C_{L_{j(n)}-(L/D)_{\max}}$, $C_{D_{j(n)}-(L/D)_{\max}}$, $(L/D)_{\max}$, λ_T and λ_Q .

$c_{j(n)}$ should be calculated before updating $(L/D)_{\max}$,

$$c_{j(n)} = \frac{2\Gamma_{j(n)}}{V_{j(n)}^* \cdot \overset{\Delta}{C}_{L_{j(n)}-(L/D)_{\max}}} \quad \dots (17)$$

where $\overset{\Delta}{C}_{L_{j(n)}-(L/D)_{\max}}$ is a frozen value and $V_{j(n)}^*$ is

$$V_{j(n)}^* = \sqrt{(V_{aj(n)} + u_{aj(n)}^*)^2 + (V_{tj(n)} + \omega_j r_{j(n)} + u_{tj(n)}^*)^2} \quad \dots (18)$$

The Reynolds number $Re_{j(n)}$ and Mach number $Ma_{j(n)}$ of the aerofoil are respectively obtained by using $c_{j(n)}$ and $V_{j(n)}^*$,

$$Ma_{j(n)} = \frac{V_{j(n)}^*}{c_a} \quad \dots (19)$$

$$Re_{j(n)} = \frac{\rho c_{j(n)} V_{j(n)}^*}{\mu} \quad \dots (20)$$

By using $Re_{j(n)}$ and $Ma_{j(n)}$, we can obtain the new $(L/D)_{\max}$ and the corresponding $C_{L_{j(n)}-(L/D)_{\max}}$, $C_{D_{j(n)}-(L/D)_{\max}}$ and $\alpha_{j(n)}-(L/D)_{\max}$ by automatically interpolating the CFD database⁽²⁴⁾. The low-Reynolds-number and high-lift airfoil S1223^(25,26) is chosen and its aerodynamics is simulated by software FLUENT in the ranges of $Re = 3,000 \sim 2.0 \times 10^7$, $Ma = 0.05 \sim 0.9$ and $\alpha = 0^\circ \sim 16^\circ$. Fig. 3 shows the contour of lift, drag and lift-drag ratio variations with Mach numbers and angles of attack at $Re = 60,000$.

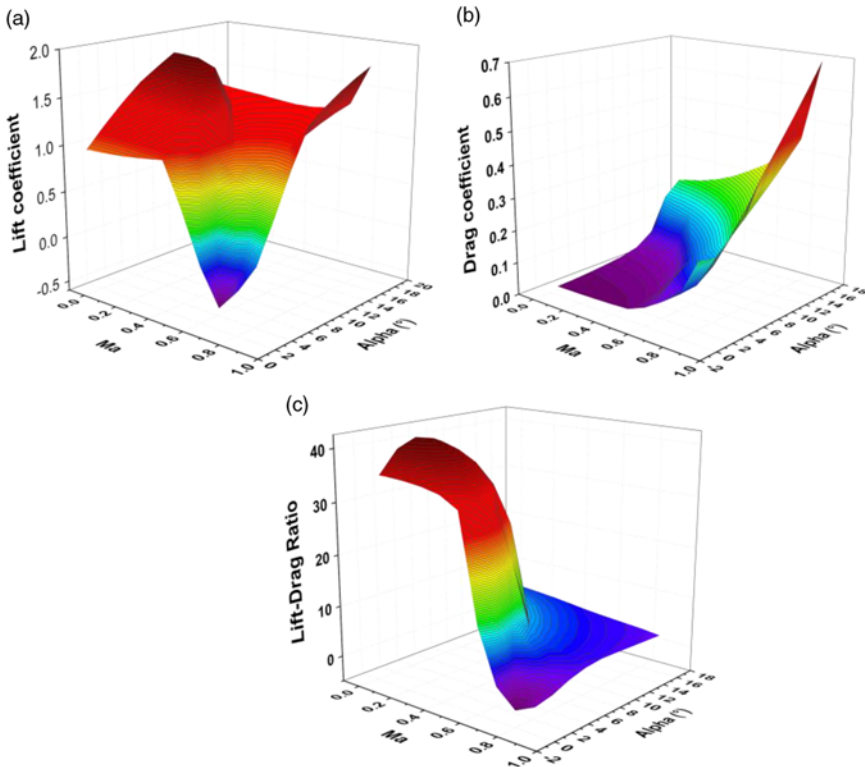


Figure 3. (a) The lift coefficient, (b) drag coefficient, (c) lift-drag ratio with variation with Mach numbers and angles of attack ($Re = 60,000$).

As is shown in Fig. 2, $\beta_{i_j(n)}$ can be written as,

$$\beta_{i_j(n)} = \arctan \left(\frac{V_a + \sum_{k=1}^2 u_{a_j,k}^*}{V_t + \omega_j r_j + \sum_{k=1}^2 u_{i_j,k}^*} \right) \dots (21)$$

And the pitch angle $\theta_{j(n)}$ is

$$\theta_{j(n)} = \alpha_{j(n)\text{-(L/D)}_{\max}} + \beta_{i_j(n)} \dots (22)$$

Finally, $\lambda_Q, \lambda_T, \Gamma_{j(n)}, \beta_{i_j(n)}$ and $c_{j(n)}$ can be iteratively optimized until all variables satisfy the prescribed convergence criterion. The framework of the present optimum design method for contra-rotating propellers is shown in Fig. 4.

3.0 VALIDATIONS

To validate the present method, computational results of thrust, torque and efficiency are compared with the CFD results. The CRP is optimized by the present approach with the following design conditions:

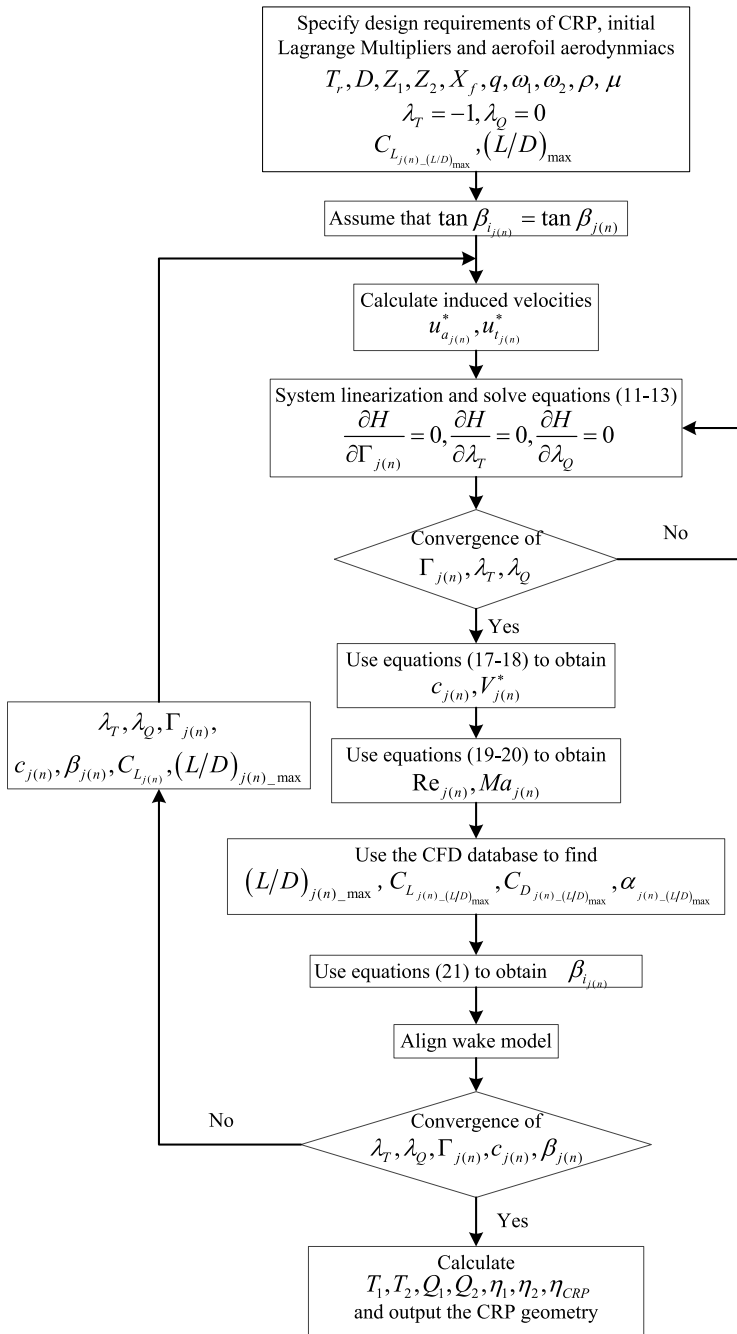


Figure 4. The framework of the present optimum design method for contra-rotating propellers.

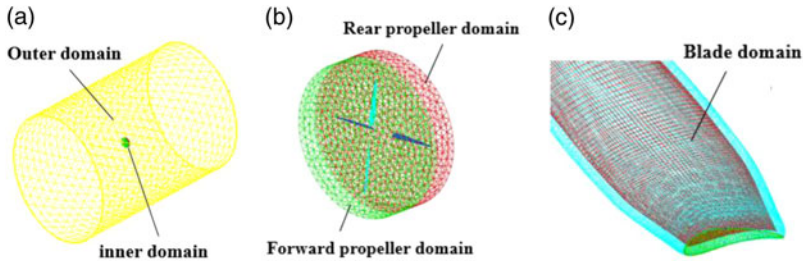


Figure 5. Computational domains of contra-rotating propeller (a) overall domain, (b) inner propeller domain, (c) blade domain.

Altitude: 20km

Air density: 0.0889 kg/m^3

Advance speed: $V_s = 20 \text{ m/s}$

Required thrust: $T_r = T_1 + T_2 = 380 \text{ N}$

Torque ratio: $q = \frac{Q_2}{Q_1} = 1$

Propeller diameter: $D = D_1 = D_2 = 5.5 \text{ m}$

Rub diameter: $0.2D$

Design advance ratio: $J_{S_1} = J_{S_2} = 0.545$

The Fluent steady RANS solver⁽²⁷⁾ is used to conduct the CFD simulations. The density-based solver is used to solve the control equations, with single precision and second order in space. The courant number is 5. The one-equation Spalart-Allmaras (S-A) turbulence model is adopted⁽²⁸⁾. The non-reflective boundary condition is set. The inlet velocity boundary condition and pressure far-field boundary condition are adopted for all simulations.

Fig. 5 shows the computational domains for simulating the flow field of contra-rotating propeller. The overall computational grid is generated with unstructured mesh and extends 20 times the radius of CRP (the cell number is 1.16 million). The mesh is divided into three parts: two inner regions for the forward propeller and the rear propeller and one outer region. The overlapping surface between different domains is defined as the interface. The boundary layer is generated and the value of Y^+ (average) is about 10. The moving reference is used to define the rotation motion of the forward and rear propeller individually. The absolute rotation speeds of the two moving references are equal to the rotation speed of the two propellers, individually. The outer domain is set to be stationary.

Note that as there is no standard model for the high-altitude contra-rotating propellers, the CFD results are used to estimate the precision of the present method. Therefore, the error mentioned below is relative to the CFD data, which is assumed to have small errors.

Fig. 6 shows the optimum chord and pitch angle distributions of CRP. It can be seen that both the optimum chord and pitch angle distributions of the forward propeller differ from that of the rear propeller.

Table 1 shows the results optimized by the present method, which are compared with the numerical results simulated by Fluent based on the configuration of the optimum CRP. In the figure, we can see that the thrust, torque and efficiency match well with the CFD data, both for the individual front and rear propellers and CRP. The optimum CRP efficiency from the present method is about 8.2% higher than that of Fluent. Since the rear propeller operates in the accelerated slipstream of the front propeller, the effective attack angle of the rear propeller is decreased. As a result, the torque (Q_2) and efficiency (η_2) of rear propeller are somewhat lower than those of front one.

Table 1
Comparisons between the results optimized by the present method and Fluent

Thrust and Torque	Present Method	Fluent
T_1/N	192.99	192.75
T_2/N	187.01	185.28
T/N (CRP)	380.00	378.03
$Q_1/(N \cdot m)$	123.63	140.14
$Q_2/(N \cdot m)$	123.62	136.73
$Q/(N \cdot m)$ (CRP)	247.25	276.87
$\eta_1/\%$	74.53	65.67
$\eta_2/\%$	72.23	64.70
$\eta/\%$ (CRP)	73.40	65.20

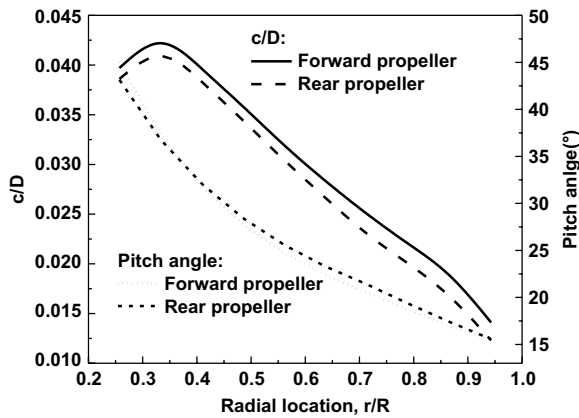


Figure 6. The optimum chord (c/D) and pitch angle distribution of the optimum CRP.

The comparisons of the propulsion performance under different advance ratios between the present method and Fluent are shown in Fig. 7. Thrust coefficients (KT), torque coefficients (KQ) and efficiency of CRP with variation of advance coefficients are given. KT and KQ are defined by

$$KT = \frac{T}{\rho n_s^2 D^4} \quad \dots (23)$$

$$KQ = \frac{Q}{\rho n_s^2 D^5} \quad \dots (24)$$

where n_s is the rotation speed per second and D is the diameter of the CRP.

It can be seen in Fig. 7 that the predicted CRP performance from the present method correlates well with the Fluent. The calculated KT curve closely matches that obtained by the Fluent, except that it is slightly underestimated at the low advance coefficients ($J_s < 0.35$). However, the calculated KQ data are somewhat lower than the CFD results. The present results of efficiency curve have the same trend with CFD, and the advance coefficient for the maximum efficiency closely matches the CFD results. Mainly due to the underprediction for torque

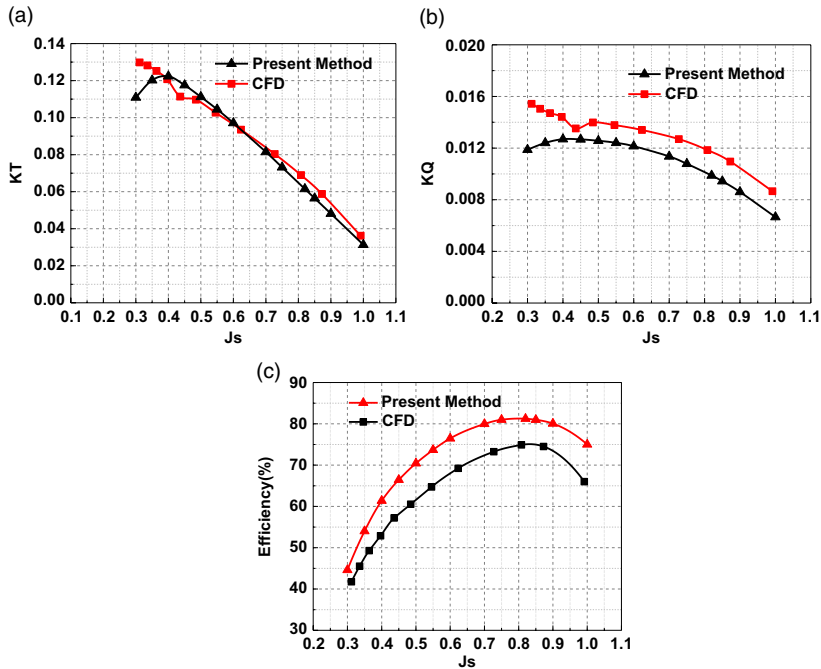


Figure 7. Comparisons of the performance under different advance ratio between the present method and CFD: (a) thrust coefficients, (b) torque coefficients, (c) efficiency of the CRP.

coefficients, the calculated results of efficiency are generally higher than the CFD results. At the advance coefficient where the maximum efficiency is achieved, it is about only 6% higher than the CFD data. The validations show that the present method can be used to optimize and analyse the efficiency of high-altitude CRPs.

4.0 RESULTS AND DISCUSSIONS

As the optimum CRP efficiency depends on both propellers, parametric studies for CRP are not the same as for the single propeller. In this section, detailed parametric studies are conducted to illustrate how the optimum efficiency of high-altitude CRP is influenced by the variations of several propeller parameters, including blade number, propeller diameter, rotation speed, axial distance and torque ratio. The thrust required on a stratosphere airship is used as the design condition. The parameters of airship and thrust for each CRP propulsion system are shown in Table 2. The hub diameters for all simulations are assumed to be 0.1 D.

4.1 Blade number

The first parametric study is to investigate the effects of blade number for each propeller. The axial distance ratio is $X_f = \frac{d}{R} = 0.3$, propeller diameter is $D_1 = D_2 = 6m$ and torque ratio is $q = \frac{Q_2}{Q_1} = 1$. The study is conducted for a range of propeller speeds, assuming both propellers rotate at the same speeds ($N_1 = N_2$).

Table 2
Parameters of airship and thrust for each CRP propulsion system

Length of Airship (m)	Volume of Airship (m ³)	Drag Coefficient of Airship	Altitude (Km)	Flight Speed (m/s)
106	89,676	0.032	20	20
Number of CRP Propulsion System		Designed Thrust of Each CRP(N)		
3		380		

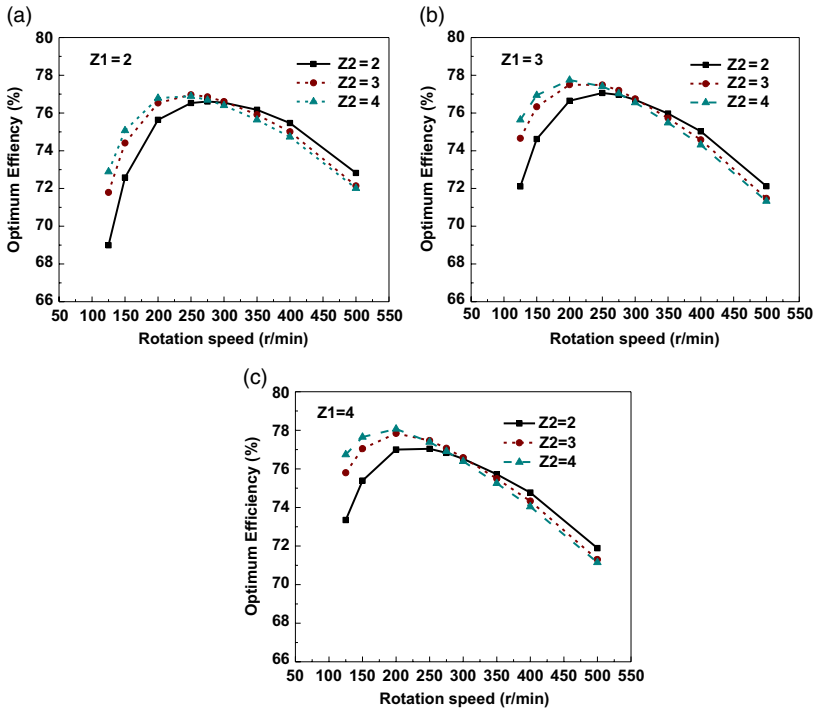


Figure 8. Optimum efficiency of CRP for different blade numbers (a) $Z_1 = 2, Z_2 = 2, 3, 4$, (b) $Z_1 = 3, Z_2 = 2, 3, 4$, (c) $Z_1 = 4, Z_2 = 2, 3, 4$.

Fig. 8 shows the optimum efficiency for different blade numbers of the forward and rear propellers. As shown in the figure, for all combinations of Z_1 and Z_2 , the optimum efficiency of the CRP first increases and then decreases with the increase of rotation speeds, with a maximal value at certain rotation speed. For a certain blade number of the forward propeller, the optimum efficiency first increases with the increase of the blade number of the rear propeller under relatively low rotation speeds ($N < 300r/min$). But then, with the increase of the rotation speed, higher optimum efficiency is found to be achieved by a lower Z_2 . This is probably because at high rotation speeds, the blade-to-blade interaction becomes stronger with Z_2 increases; thus, the performance of CRPs deteriorates and the efficiency decreases.

The most efficient CRP configurations with respect to the number of blades are summarized in Table 3. The combination of blade numbers $Z_1 = 4, Z_2 = 4$ achieves the highest efficiency of 78.07%, which is 1.46% higher than the configuration of $Z_1 = Z_2 = 2$. However, considering

Table 3
The optimal efficiency for different combinations of front and rear propeller blade numbers

Z_1	Z_2	Optimal Efficiency (%)
2	2	76.61
2	3	76.97
2	4	76.89
3	2	77.75
3	3	77.50
3	4	77.75
4	2	77.04
4	3	77.84
4	4	78.07

that more blades are required for the former configuration, the structure weights as well as manufacturing cost and difficulty will be higher. Therefore, a trade-off analysis on the choice of combinations of blade number needs to be conducted in the engineering design of the CRP propulsion system for high-altitude airships. In the following parametric studies, the configuration of $Z_1 = Z_2 = 2$ is chosen for all cases.

4.2 Diameter and rotation speed

For the CRP propulsion system of the HAAs, the two propellers can be driven by two individual motors; thus, there is no requirement that the two propellers must rotate at the same speeds. In Section 4.1 the assumptions of diameters keeping unchanged and both propellers rotating at the same speed are adopted. In this section, however, there is no constraint for both propellers rotating at the same speed and diameter keeping constant, so the effects of different configurations will be analysed for a range of propeller speeds and diameters. Figure 8 shows the optimum efficiency of CRPs under different diameters, varying with rotation speeds of the front propeller and the rear propeller. The horizontal axis represents the forward propeller rotation speed (N_1), and the vertical axis represents the rear propeller rotation speed (N_2).

It can be seen in Fig. 9 that for each diameter, the optimum efficiency has a maximal value with the variation of N_1 and N_2 . It can be seen that the optimum efficiency is highly affected by the diameter. The maximum efficiency generally increases with the increases of diameter. And it is interesting to see that even though there is no constraint that the forward and rear propellers rotate at the same rotation speeds, the maximum efficiency for each diameter is consistently achieved when both propellers are rotating at the same speed ($N_1 = N_2$). And the optimum rotation speeds decrease with the increases of diameter. The maximum efficiency of 76.61% is achieved at $D = 6m$, $[N_1, N_2] = [275\text{rpm}, 275\text{rpm}]$. Besides, it is observed that, at a certain diameter, the optimum efficiency is not significantly affected by the rotation speed difference of the two propellers. For example, when $D = 6m$ and $N_1 = 350\text{rpm}$, the optimal efficiency 76.43% is achieved at $N_2 = 250\text{rpm}$, while the efficiency is 76.17% at $N_2 = N_1 = 350\text{rpm}$, which is only 0.26% lower than the optimal value. However, the difference of design rotation speeds between the forward and rear propellers indicates different design conditions for the development of driving motors, leading to the requirement of two different motors for a CRP propulsion system. Therefore, if the optimum design rotation speeds of the

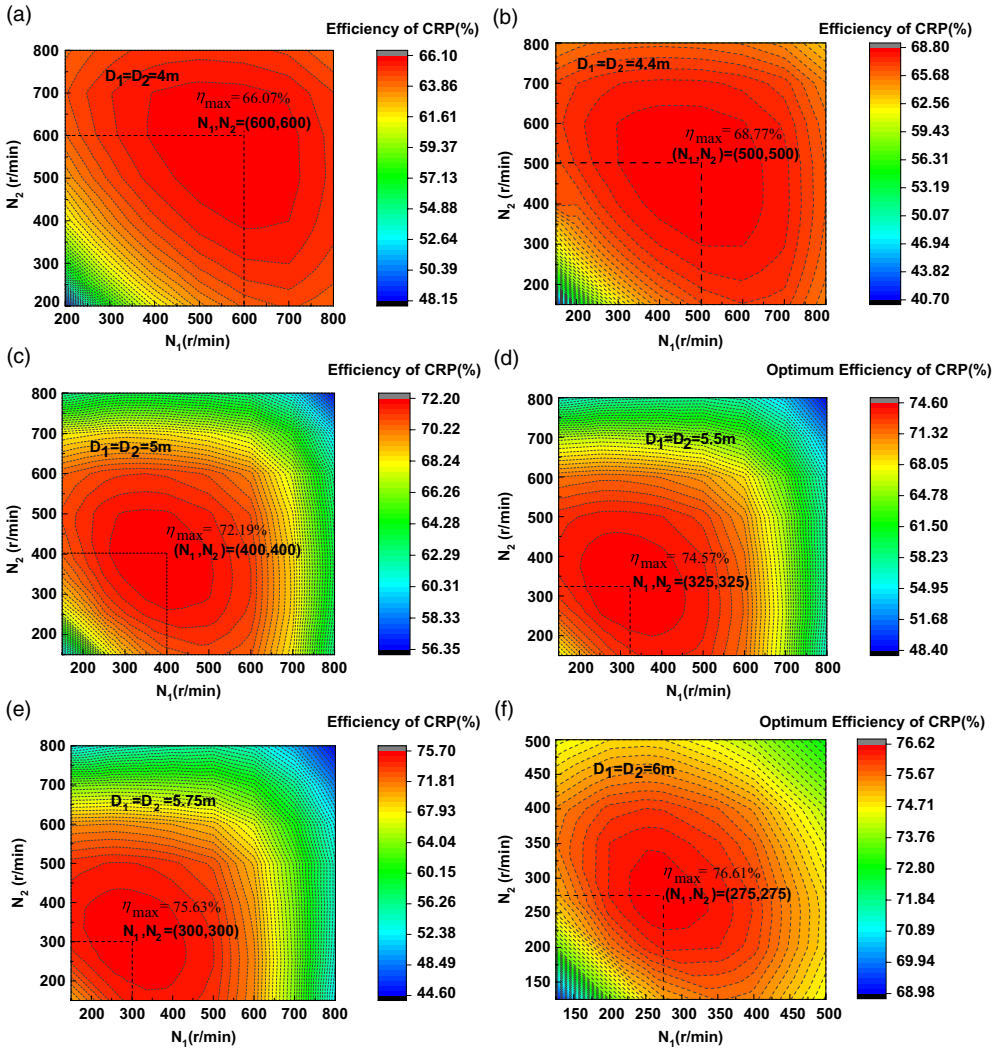


Figure 9. Optimum efficiency of CRP for different propeller diameter.

two propellers are found to be different ($N_1 \neq N_2$), which makes the CRP system more expensive or complicated, we can probably design the two propellers rotating at the same rotation speeds without significantly decreasing the efficiency of CRP.

Fig. 10 shows the optimum efficiency of CRP for different propeller diameters, where both propellers are rotating at the same speeds. It can be seen that the optimum efficiency has a maximal value at a certain rotation speed. However, the maximal efficiency has no significant difference with that achieved at the neighbouring rotation speeds. Fig. 11 shows the optimum efficiency of CRP for different design rotation speeds. We can see that, under different design rotation speeds, the effects of the diameter on the optimum efficiency are not consistent. In the present design region of diameter, when $N = 250\text{rpm}$ and $N = 600\text{rpm}$, the increase of diameter is totally beneficial to the optimum efficiency; when $N = 700\text{rpm}$, a maximal efficiency is obtained at $D = 5\text{m}$; and when $N = 800\text{rpm}$, the optimum efficiency decreases with

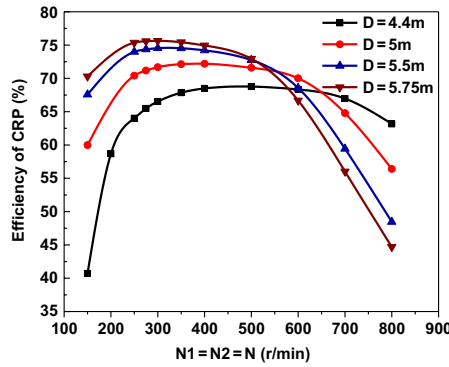


Figure 10. Optimum efficiency of CRP for different propeller diameters.

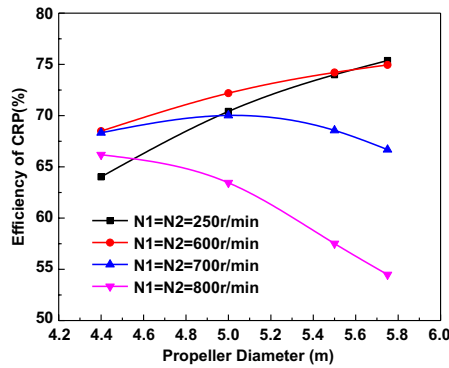


Figure 11. Optimum efficiency of CRP for different design rotation speeds.

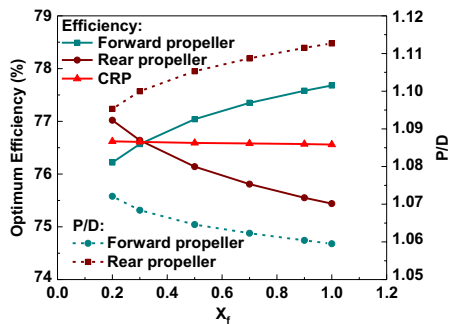


Figure 12. Optimum efficiency and pitch ratio variations with the axial distance between the front propeller and rear propeller.

the increases of diameter. Sometimes, high-altitude CRP propulsion systems are designed with limited available selections of driving motors whose optimal rotation speeds are certain. Under this prescribed design condition, the diameter of CRP needs to be suitably designed to achieve high efficiency.

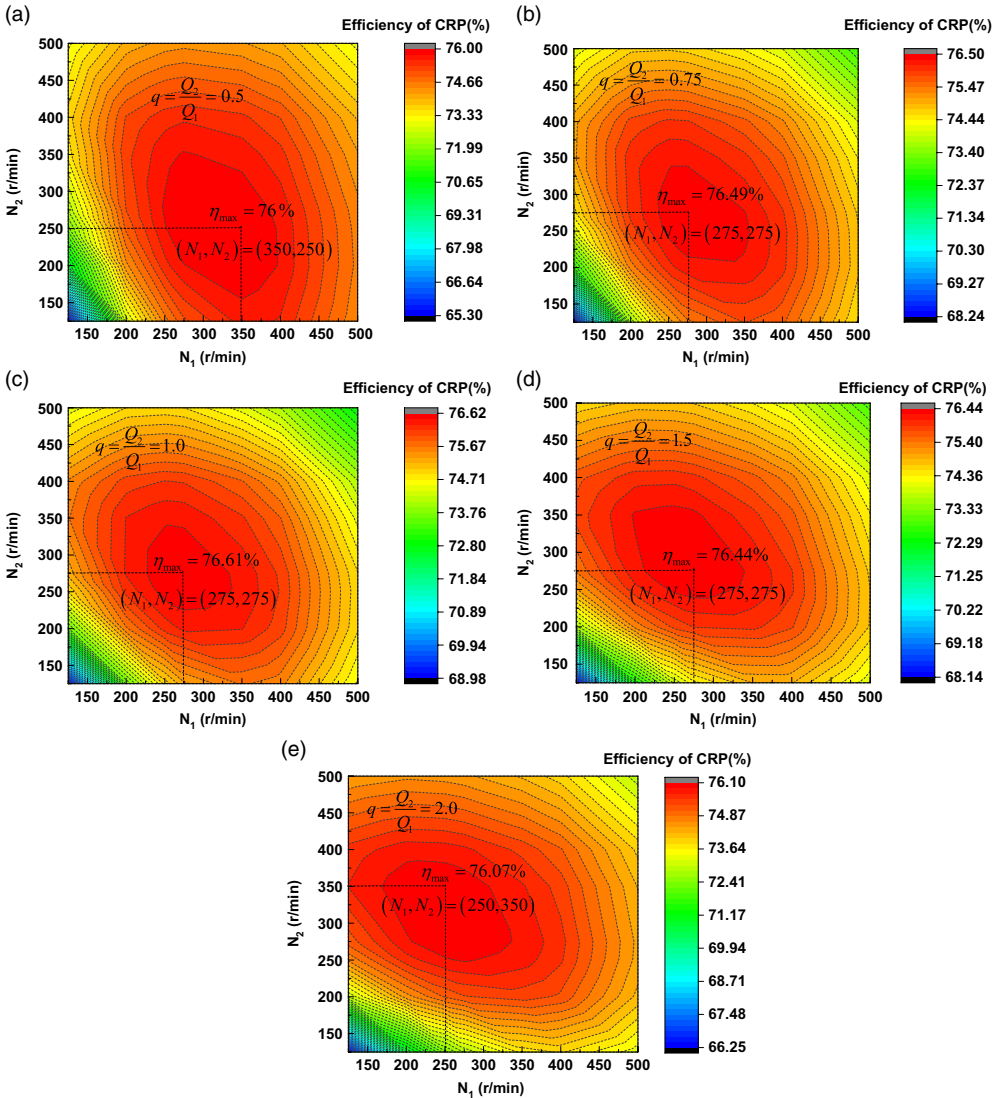


Figure 13. Optimum efficiency of CRP for different torque ratios.

4.3 Axial distance

In the parametric analysis in the previous sections, the axial distance $d = 0.3R$ ($X_f = \frac{d}{R} = 0.3$) between the front and rear propellers were assumed for all optimization cases. This section will investigate the effects of different axial distances on the CRP optimum efficiency. The other parameters of the CRP used here are chosen based on the parametric studies in section 4.1 and section 4.2. ($Z_1 = Z_2 = 2$, $D = 6\text{m}$, $N_1 = N_2 = 275\text{rpm}$). Only the axial distance is allowed to vary with X_f ranging from 0.2 to 1.0. The optimum CRP efficiency varying with X_f is shown in Fig. 12. The geometric pitch ratio P_D at $r = 0.75R$ ($P_D = \frac{P}{D} = \frac{2\pi r_{0.75} \tan \beta_{i0.75}}{D}$) for both propellers is also given in the figure.

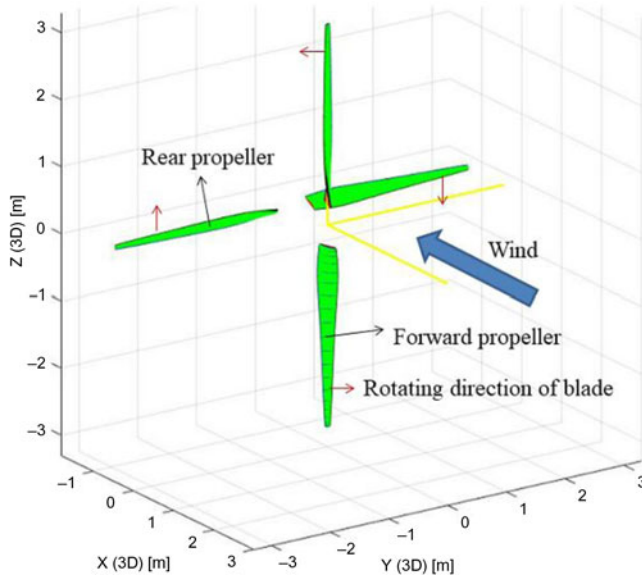


Figure 14. The three-dimensional configuration of the contra-rotating propeller finally designed.

In the figure, we can see that the axial distance has obvious effects on the individual efficiency of each propeller. The efficiency of the forward propeller increases with the increases of X_f , mainly because lower axial velocity is induced by the rear propeller, resulting in a lower required P_D . Conversely, with the increases of X_f due to higher axial velocity induced by the forward propeller, the efficiency increases and the required P_D decreases for the rear propeller. When X_f is relatively small ($X_f < 0.3$), the rear propeller efficiency is higher than that of forward propeller while it is contrary for higher X_f . However, as shown in the figure, the total optimum CRP efficiency is slightly affected by the variation of X_f .

4.4 Torque ratio

In previous sections, the prescribed torque for both propellers were assumed to be equal (torque ratio $q = \frac{Q_2}{Q_1} = 1$). In this section, the effects of this parameter on the optimum efficiency will be investigated. The torque ratio is allowed to be changed from 0.5 to 2.0.

Fig. 13 shows the optimum efficiency of CRP for different torque ratios. As shown in the figure, it is interesting to find that the maximum efficiency is achieved when $q = 1.0$, even without the constraint of both propellers having the same torque. This is probably because when $q = 1.0$, the aerodynamic loads on both propellers are very close under the same rotation speed, and the tangential interaction induced velocity on the rear propeller induced by the forward propeller can exactly counteract its self-induced velocity. Therefore, the rear propeller can most efficiently recover the rotational energy losses originating from the forward propeller in this case. However, the efficiency has no significant difference under a different torque ratio. The maximum efficiency is about 76.61% when $q = 1.0$, which is 0.61% higher than the lowest value of 76.0% when $q = 0.5$. Considering that the maximum efficiency is achieved at same torque and rotation speeds for both propellers, it is beneficial to the design of a high-altitude CRP propulsion system, especially for reducing the complexity of motor design.

The three-dimensional configuration of the contra-rotating propeller finally designed is shown in Fig. 14.

5.0 CONCLUSIONS

The efficiency of high-altitude contra-rotating propellers will significantly affect the overall performance of stratosphere airship. An improved optimization algorithm based on the vortex lifting line method is established in designing the high-altitude CRPs. The chord length and pitch distributions for the forward and rear propeller are obtained by coupling optimization with considering the radial variation of Reynolds numbers and Mach numbers. The improved approach is validated by CFD method. The optimization results for a high-altitude CRP show a good agreement with CFD, indicating that the method can be used as an efficient tool to select the CRPs in the preliminary stage of stratosphere aircraft design. Besides, by conducting detailed parametric optimizations, the effects of rotation speeds, propeller diameter, blade number, axial distance and torque ratio on the optimum efficiency are illustrated in detail, which are helpful to the design of high-altitude CRPs. Assuming no constraint for the design rotation speeds, the diameter and blade numbers affect the optimum efficiency in a relatively high degree while the effects of axial distance and torque ratio is relatively lower. Some main conclusions include:

1. For a certain blade number of the forward propeller, the optimum efficiency first increases with the increase of the blade number of the rear propeller. But then, with the increase of the rotation speed, higher optimum efficiency is achieved by a lower blade number of the rear propeller. And a trade-off analysis on the choice of blade numbers for high-altitude CRPs needs to be conducted, considering the efficiency, structure weights, manufacturing cost and difficulty.
2. The diameter highly affects the optimum efficiency of CRPs. The maximum efficiency generally increases with the increases of the diameter. The maximum efficiency for each diameter is achieved when both propellers rotate at the same speed. Besides, under different design rotation speeds, the effects of the diameter on the optimum efficiency are not consistent. Therefore, in the case that the choice of available motor is determined in advance whose design rotation speed is certain, the diameter of CRP needs to be suitably designed to achieve high efficiency.
3. The axial distance has obvious effects on the individual efficiency of both the front and rear propellers, mainly because of the mutually induced velocity between the two propellers. However, the total optimum CRP efficiency is slightly affected by the variation of the axial distance. (The range considered for axial distance ratio between front and rear propellers is 0.3 to 1.0 in this paper.)
4. The maximum efficiency is achieved when the two propellers have same torque. This is probably because when the torque is equal, the tangential interaction induced velocity on rear propeller induced by the forward propeller can exactly counteract its self-induced velocity. Therefore, the rear propeller can most efficiently recover the rotational energy losses originating from the forward propeller. It is beneficial to the design of a high-altitude CRP propulsion system, especially for reducing the complexity of motor design.

ACKNOWLEDGEMENTS

This research was supported by the National Natural Science Foundation of China [Grant NO. 61733017] and China Postdoctoral Science Foundation [Grant NO. 2017M621480]. Also, the authors offer special thanks to the reviewers for their valuable comments and suggestions, which are very helpful to improve this paper.

REFERENCES

1. JAMISON, L., SOMMER, G.S. and PORCHE, I.R. *High-Altitude Airships for the Future Force Army*, Rand Arroyo Center TR-234-A, 2005, Santa Monica, CA.
2. COLOZZA, A. Initial feasibility assessment of a high altitude long endurance airship. NASA CR-2003-212724, 2003.
3. LIU, P.Q., DUAN, Z., MA, L. and MA, R. Aerodynamics properties and design method of high efficiency-light propeller of stratospheric airships. *Int Conf Remote Sens, Environ Transp Eng*, June 2011, pp 8041–8044. doi:10.1109/RSETE.2011.5964019.
4. LIU, P.Q., TANG, Z.H., CHEN, Y.X. and GUO, H. Experimental feasibility assessment of counter-rotating propellers for stratospheric airships. 53rd AIAA Aerospace Sciences Meeting, AIAA 2015–1019, January 2015. doi:10.2514/6.2015-1029.
5. XU, J.H., SONG, W.P., YANG, X.D. and ZHANG, Y. Investigation on improving efficiency of high-altitude propeller with tandem configuration. 35th AIAA Applied Aerodynamics Conference, AIAA 2017–3575, June 2017. doi:10.2514/6.2017-3575.
6. ZHA, G.C., CARROLL, B.F., PAXTON, C.D. and CONLEY, C.A. High-performance airfoil using coflow jet flow control, *AIAA J*, 2007, **45**, (8), pp 2087–2090. doi:10.2514/1.20926.
7. CHENG, Y.F., CHE, X.K. and NIE, W.S. Numerical study on propeller flow-separation control by DBD-plasma aerodynamic actuation, *IEEE Trans Plasma Sci*, April 2013, **41**, (4), pp 892–898. doi:10.1109/TPS.2013.2248384.
8. XU, J.H., SONG, W.P. and YANG, X.D. Effects of proplet on propeller efficiency, *Am Inst Phy Conf Series*, September 2011, **1376**, (1), pp 165–168. doi:10.1063/1.3651864.
9. TANG, Z.H., LIU, P.Q., CHEN, Y.X. and GUO, H. Experimental study of counter-rotating propellers for high-altitude airships, *J Propul Power*, 2015, **31**, (5), pp 1491–1496. doi:10.2514/1.B35746.
10. BIERMANN, D. and GRAY, W.H. Wind-tunnel tests of single- and dual-rotating pusher propellers having from three to eight blades, NACA ARR-(WR-L-359), February 1942.
11. PAIK, K.J., HWANG, S., JUNG, J., LEE, T. and LEE, Y.Y. Investigation on the Wake Evolution of contra-rotating propeller using RANS computation and SPIV measurement, *Inter J Naval Archit Ocean Eng*, 2015, **7**, (3), pp 595–609. doi:10.1515/ijnaoe-2015-0042.
12. XIN, G.Z., DING, E.B. and TANG, D.H. A design method for contra-rotating propeller by lifting-surface method, *J Ship Mech*, April 2006, **10**, (2), pp 40–46 (in Chinese).
13. BIERMANN, D. and HARTMAN, E.P. Wind-tunnel tests of four- and six-blade single- and dual-rotating tractor propellers, *NACA Rept*, 1942, **28**, (747).
14. MCHUGH, J.G. and PEPPER, E. The characteristics of two model six-blade counter-rotating pusher propellers of conventional and improved aerodynamic design, NACA ARR-(WR-L-404), June 1942.
15. CONEY, W.B. A Method for the Design of a Class of Optimum Marine Propellers, PhD dissertation, Massachusetts Institute of Technology, Cambridge, Massachusetts, 1989.
16. EPPS, B., CHALFANT, J., KIMBALL, R., TECHET, A. and CHRYSOSTOMIDIS, C. OpenProp: An open-source parametric design and analysis tool for propellers, 2009 Grand Challenges in Modeling & Simulation Conference, Istanbul, Turkey, 2009, pp 104–111.
17. EPPS, B.P. and KIMBALL, R.W. Unified rotor lifting line theory, *J Ship Res*, December 2013, **57**, (4), pp 181–201. doi:10.5957/JOSR.57.4.110040.
18. LERBS, H.W. Moderately loaded propellers with a finite number of blades and an arbitrary distribution of circulations, *Trans Soc Naval Archit Marine Eng*, 1952, **60**, pp 73–123.
19. MORGAN, W. The design of counterrotating propellers using Lerbs' theory, *Trans Soc Naval Archit Marine Eng*, 1960, **68**, pp 6–38.
20. MORGAN, B.M. and WRENCH, J.W. Some computational aspects of propeller design, *Method Comput Phy*, 1965, **4**, pp 301–331.
21. KERWIN, J.E., CONEY, W.B. and HSIN, C.Y. Optimum circulation distributions for single and multi-component propellers, Twenty-First American Towing Tank Conference, Washington, DC, August 1986, pp 53–62.
22. LASKOS, D. *Design and Cavitation Performance of Contra-rotating Propeller*, SM thesis, Massachusetts Institute of Technology, Cambridge, Massachusetts, 2010.
23. EPPS, B.P. *An Impulse Framework for Hydrodynamic Force Analysis: Fish Propulsion, Water Entry of Spheres, and Marine Propellers*, PhD thesis, Massachusetts Institute of Technology, Cambridge, Massachusetts, 2010.

24. ZHENG, X.K., WANG, X.L., CHENG, Z.J. and HAN, D. The efficiency analysis of high-altitude propeller based on vortex lattice lifting line theory, *Aeronaut J*, February 2017, **121**, (1236), pp 141–162. doi:[10.1017/aer.2016.112](https://doi.org/10.1017/aer.2016.112).
25. SELIG, M.S. and GUGLIELMO, J.J. High-lift low Reynolds number airfoil design, *J Aircraft*, January 1997, **34**, (1), pp 72–79. doi:[10.2514/2.2137](https://doi.org/10.2514/2.2137).
26. MA, R. and LIU, P.Q. Numerical simulation of low-Reynolds-number and high-lift airfoil S1223, Proceedings of the World Congress on Engineering 2009, WCE 2009, London, July 2009, **2**, pp 1691–1696.
27. FLUENT Software Package, Ver 6.3.26, FLUENT Inc., 2006.
28. SPALART, P.R. and ALLMARCHAS, S.R. A one-equation turbulence model for aerodynamic flows, 30th Aerospace Sciences Meeting and Exhibit, AIAA Paper 92–0439, Reno, NV, U.S.A, January 1992. doi:[10.2514/6.1992-439](https://doi.org/10.2514/6.1992-439).